

Transport of indirect excitons and exciton mediated spin transport in a van der Waals heterostructure in magnetic fields

Zhiwen Zhou, W. J. Brunner, E. A. Szwed, L. H. Fowler-Gerace, and L. V. Butov

Department of Physics, University of California San Diego, La Jolla, CA, USA

(Dated: January 21, 2026)

We studied transport of indirect excitons (IXs) and IX mediated spin transport in a $\text{MoSe}_2/\text{WSe}_2$ van der Waals heterostructure in magnetic fields up to 8 T. We observed the long-range IX transport and the long-range IX mediated spin transport in the magnetic fields. The IX transport and spin transport are characterized by the $1/e$ decay distances reaching ~ 100 micrometers. The decay distance of the spin transport correlates with the decay distance of IX transport. These decay distances first increase and then decrease with increasing IX density for all studied magnetic fields. The long-range IX transport and the long-range spin transport in the magnetic fields are consistent with the similar long-range transport in zero magnetic field.

INTRODUCTION

Spatially indirect excitons (IXs), also known as inter-layer excitons, are composed from electrons and holes in separated layers in a heterostructure (HS) [1]. Due to the separation between the electron and hole layers, IX lifetimes exceed lifetimes of regular spatially direct excitons (DXs) by orders of magnitude [2]. The long lifetimes, enable IX transport over long distances and also allow IXs to form the Bose-Einstein condensate [3].

In addition to the long-range exciton transport, IXs also enable long-range spin transport. Scattering of particles carrying the spin states can cause the spin relaxation that limits the spin transfer [4]. Therefore, the suppression of scattering in IX condensate can suppress the spin relaxation caused by scattering. In addition, the electron-hole separation in IXs suppresses the spin relaxation caused by electron-hole exchange [5]. Therefore, traveling IXs can efficiently transfer spin states, allowing the realization of long-range spin transport.

IX transport is studied in various materials, including GaAs HS [6–21], GaN HS [22], and ZnO HS [23]. IX mediated spin transport in GaAs HS is also explored [24–28]. Recently, studies of IX transport and IX mediated spin transport were started in van der Waals HS composed of atomically thin layers of transition metal dichalcogenides (TMD). TMD HS offer a unique materials platform for studying exciton transport and exciton mediated spin transport. Both DXs in TMD HS [29–31] and IXs in TMD HS [32, 33] have high binding energies reaching hundreds of meV, significantly higher than IX binding energies in HS formed from III-V or II-VI semiconductors that reach 3–4 meV in GaAs/AlGaAs HS [34, 35], 10 meV in AlAs/GaAs HS [2], and 30 meV in ZnO HS [36]. Due to the high binding energies, IXs in TMD HS are stable at room temperature. Furthermore, the superfluidity temperature, which can be achieved with excitons, is proportional to the exciton binding energy and the high IX binding energies in TMD HS give an opportunity to realize high-temperature superfluidity [32]. IXs in peri-

odic moiré potentials in TMD HS also allow exploring the Bose-Hubbard physics [37–51].

DX transport [52–58], IX transport [59–79], DX mediated spin transport [80], and IX mediated spin transport [59, 62, 65, 69] are intensively studied in TMD materials. (Due to the coupling of the spin and valley indices [81–84] the spin transport is coupled to the valley transport in TMD HS and, therefore, for simplicity, we will use the term ‘spin’ also for ‘spin-valley’.) These studies showed that in-plane disorder suppress diffusive IX transport and IX mediated spin transport due to IX localization and scattering: In TMD HS, even in the case of long IX lifetimes, diffusive IX transport [59–75] and IX mediated spin transport [59, 62, 65, 69] are characterized by low $1/e$ decay distances $d_{1/e}$ and $d_{1/e}^s$, respectively, up to a few micrometers. Recent studies showed that long-range IX transport and long-range IX mediated spin transport with $d_{1/e}$ and $d_{1/e}^s$ reaching 100 micrometers can be realized in TMD HS [85, 86].

In this work, we studied IX transport and IX mediated spin transport in a $\text{MoSe}_2/\text{WSe}_2$ van der Waals HS in magnetic fields up to 8 T. The dispersion relation of excitons in high magnetic fields was theoretically studied for three-dimensional (3D) excitons [87], 2D excitons in a perpendicular magnetic field [88–90], and IXs in a perpendicular magnetic field [91]. It was shown that high magnetic fields induce coupling between the exciton internal structure and c.m. motion [87–91]. This coupling modifies the exciton dispersion and enhances the exciton mass that was measured for IXs in GaAs/AlGaAs HS in Refs. [92, 93]. The studies of IX transport in GaAs/AlGaAs HS showed a strong reduction of IX transport distance with increasing magnetic field [94, 95]. In this work, we probe the effect of magnetic field on IX transport in van der Waals TMD HS.

EXPERIMENT

We consider IX transport in $\text{MoSe}_2/\text{WSe}_2$ HS where adjacent MoSe_2 monolayer and WSe_2 monolayer form

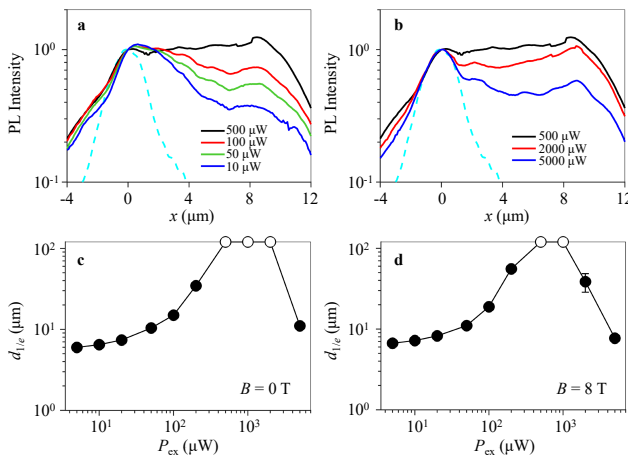


FIG. 1: IX transport in magnetic fields. (a,b) Normalized LE-IX luminescence profiles in magnetic field $B = 8$ T for laser excitation power $P_{\text{ex}} = 500, 100, 50, 10 \mu\text{W}$ (top to bottom) in (a) and $P_{\text{ex}} = 500, 2000, 5000 \mu\text{W}$ (top to bottom) in (b). The dashed line shows the DX luminescence profile in the MoSe₂ monolayer; this profile is close to the laser excitation profile for short-range DX transport. The $\sim 2 \mu\text{m}$ laser spot is centered at $x = 0$. (c,d) The $1/e$ decay distance of IX transport $d_{1/e}$ vs. P_{ex} for magnetic field $B = 0$ (c) and 8 T (d). The $d_{1/e}$ values are obtained from least-squares fitting the LE-IX luminescence profiles to exponential decays in the region $x = 0 - 9 \mu\text{m}$, from the excitation spot to the HS edge. The data with the fit indicating diverging $d_{1/e}$ are presented by circles on the edge.

the separated electron and hole layers for IXs [96]. The HS details are presented in Appendix A.

IXs are generated by focused laser excitation with the laser excitation energy resonant to DX in WSe₂ HS layer. As shown in Ref. [85], the resonant excitation enhances the IX transport distances. As in earlier studies [59–79, 85], the propagation of the IX PL intensity from the laser excitation spot is measured via spatially-resolved imaging to characterize the IX transport. In turn, as in earlier studies [59, 62, 65, 69, 86], the propagation of the circularly polarized IX PL intensity from the laser excitation spot is measured via spatially- and polarization-resolved imaging to characterize the IX mediated spin transport. The measurement details are presented in Appendix B.

Figure 4 in Appendix C shows IX PL spectra at different laser excitation powers P_{ex} . The spectra at zero magnetic field (Fig. 4b,e,h) are similar to the corresponding zero-field spectra considered in Ref. [86]: A single lower-energy IX (LE-IX) line is observed in the spectra at low P_{ex} and an additional higher-energy IX (HE-IX) line appears in the spectra at high P_{ex} . The HE-IX line was attributed to the appearance of moiré cells with double occupancy in Ref. [86]. Figure 4 shows that similar IX spectra are observed in the studied magnetic fields $-8 \text{ T} < B < 8 \text{ T}$. In this work, we consider the propagation of the LE-IX PL intensity from the laser excitation spot to characterize the IX transport (Figs. 1-3). The LE-IX spectra are separated from the HE-IX spectra by the Gaussian fits (Fig. 4). Figure 5 in Appendix D shows that considering the spectrally integrated IX PL intensity gives qualitatively similar IX transport characteristics.

Figures 1a,b show LE-IX PL profiles $I(x)$ in magnetic field $B = 8$ T for different laser excitation power P_{ex} . IXs propagate from the laser excitation spot centered at $x = 0$. The excitation spot is presented in Figs. 1a,b by the DX luminescence profile in the MoSe₂ monolayer; this profile is close to the laser excitation profile for short-range DX transport. The IX transport from the excitation spot is quantified by the $1/e$ decay distance of LE-IX PL $d_{1/e}$. The $d_{1/e}$ values are obtained from least-squares fitting the LE-IX luminescence profiles $I(x)$ to exponential decays in the region $x = 0 - 9 \mu\text{m}$, from the excitation spot to the HS edge.

For zero magnetic field, the IX transport enhances with increasing P_{ex} for $P_{\text{ex}} \lesssim 500 \mu\text{W}$ and reduces with increasing P_{ex} for higher P_{ex} as shown by the variation of $d_{1/e}$ with P_{ex} in Fig. 1c. A similar dependence of IX transport on the excitation density was observed in earlier studies in zero magnetic field in Ref. [85].

IX transport in magnetic fields also non-monotonically depends on density (Fig. 1a,b), with $d_{1/e}$ first increasing and then reducing with P_{ex} (Fig. 1d). Furthermore, the long-range IX transport with $d_{1/e}$ reaching $100 \mu\text{m}$ is realized in magnetic fields (Fig. 1d).

IX signal vanishes outside HS and, for the fit of the data in the HS range $x = 0 - 9 \mu\text{m}$, from the excitation spot to the HS edge, the uncertainties in the fit allow determining $d_{1/e}$ up to $\sim 100 \mu\text{m}$: For $d_{1/e} \lesssim 100 \mu\text{m}$, the uncertainties in the fit (shown by the error bars when larger than the point size in Fig. 1c,d) are small; however, for $d_{1/e}$ extracted from the fit higher than $\sim 100 \mu\text{m}$, the uncertainties become large and comparable to the extracted $d_{1/e}$.

IX transport considered above is characterized by the propagation of total IX PL intensity in both circular polarizations $n \sim I_{\sigma^+} + I_{\sigma^-}$, where I_{σ^+} is the intensity of IX PL co-polarized with the circularly polarized laser excitation and I_{σ^-} is the intensity of cross-polarized IX PL. The degree of circular polarization of IX PL $P = (I_{\sigma^+} - I_{\sigma^-})/(I_{\sigma^+} + I_{\sigma^-})$. The transport of spin polarization density carried by IXs is characterized by the propagation of $I_{\text{spin}} = Pn = I_{\sigma^+} - I_{\sigma^-}$. Figures 2a,b show LE-IX spin density profiles $I_{\text{spin}}(x)$ in magnetic field $B = 8$ T for different P_{ex} . The IX mediated spin transport from the excitation spot is quantified by the $1/e$ decay distance of spin density profiles $d_{1/e}^s$. The $d_{1/e}^s$ values are obtained from least-squares fitting the $I_{\text{spin}}(x)$ profiles to exponential decays in the region $x = 0 - 9 \mu\text{m}$, from the excitation spot to the HS edge.

For zero magnetic field, the IX mediated spin transport enhances with increasing P_{ex} for $P_{\text{ex}} \lesssim 500 \mu\text{W}$ and

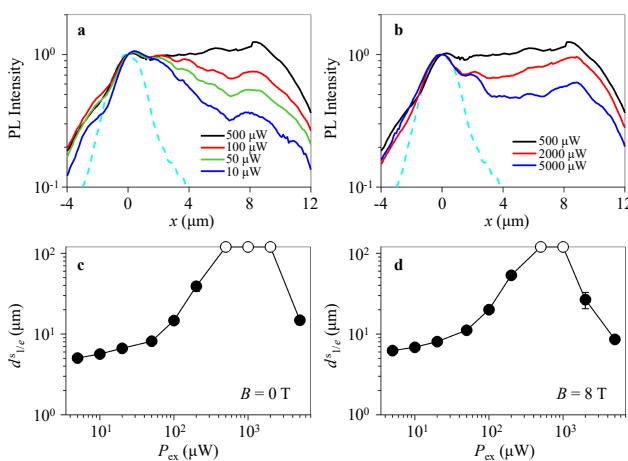


FIG. 2: IX mediated spin transport in magnetic fields. (a,b) Normalized LE-IX spin density profiles $I_{\text{spin}} = I_{e+} - I_{e-}$ in magnetic field $B = 8$ T for laser excitation power $P_{\text{ex}} = 500, 100, 50, 10 \mu\text{W}$ (top to bottom) in (a) and $P_{\text{ex}} = 500, 2000, 5000 \mu\text{W}$ (top to bottom) in (b). The dashed line shows the DX luminescence profile in the MoSe₂ monolayer; this profile is close to the laser excitation profile for short-range DX transport. The $\sim 2 \mu\text{m}$ laser spot is centered at $x = 0$. (c,d) The $1/e$ decay distance of IX mediated spin density transport $d_{1/e}^s$ vs. P_{ex} for magnetic field $B = 0$ (c) and 8 T (d). The $d_{1/e}^s$ values are obtained from least-squares fitting the $I_{\text{spin}}(x)$ profiles to exponential decays in the region $x = 0 - 9 \mu\text{m}$, from the excitation spot to the HS edge. The data with the fit indicating diverging $d_{1/e}^s$ are presented by circles on the edge.

reduces with increasing P_{ex} for higher P_{ex} as shown by the variation of $d_{1/e}^s$ with P_{ex} in Fig. 2c. A similar dependence of IX mediated spin transport on the excitation density was observed in earlier studies in zero magnetic field in Ref. [86].

IX mediated spin transport in magnetic fields also non-monotonically depends on density (Fig. 2a,b), with $d_{1/e}^s$ first increasing and then reducing with P_{ex} (Fig. 2d). Furthermore, the long-range spin transport with $d_{1/e}^s$ reaching $100 \mu\text{m}$ is realized in magnetic fields (Fig. 2d). As for the IX transport decay distance $d_{1/e}$ outlined above, the uncertainties in the fit allow determining the spin transport decay distance $d_{1/e}^s$ up to $\sim 100 \mu\text{m}$.

We measured IX transport and IX mediated spin transport for magnetic fields $-8 \text{ T} < B < 8 \text{ T}$. For all studied magnetic fields, the IX transport decay distance $d_{1/e}$ (Fig. 3a) and spin transport decay distance $d_{1/e}^s$ (Fig. 3b) reach $\sim 100 \mu\text{m}$. Both $d_{1/e}$ and $d_{1/e}^s$ first increase and then decrease with increasing IX density for all studied magnetic fields (Fig. 3a,b).

Figure 3c presents the correlation between $d_{1/e}$ and $d_{1/e}^s$. The values for $d_{1/e}$ and $d_{1/e}^s$ in Fig. 3c are taken from Fig. 3a and Fig. 3b. Figure 3c shows that the decay distance of the spin transport correlates with the decay

distance of the IX transport. The enhancement of $d_{1/e}^s$ with $d_{1/e}$ is observed in a broad range of both excitation density and magnetic field variations, corresponding to the range of these parameters in Figs. 3a,b.

DISCUSSION

IX transport. For diffusive IX transport in a disordered in-plane potential in a heterostructure, the IX transport decay distance $d_{1/e}$ increases with density due to the enhancement of IX screening of the disorder potential and the enhancement of repulsive interaction between IXs [10, 13, 102]. However, for the IX long-range transport, a different behavior is observed: $d_{1/e}$ drops with density at high densities (Fig. 1c). The disagreement with the diffusive IX transport is outlined in the studies of the IX long-range transport in $B = 0$ in Ref. [85].

The Bose-Hubbard model predicts the superfluid phase for the number of bosons per lattice site $N \sim 1/2$ and the insulating phase (Mott insulator or the Bose glass) for $N \sim 0$ and $N \sim 1$ [103]. The IX long-range transport and the enhancement followed by the suppression of $d_{1/e}$ with density (Fig. 1d) are consistent with this prediction. For the IX long-range transport, the mean-field estimate for the IX density $n = \varepsilon \delta E / (4\pi e^2 d_z)$ [104] gives $n \sim 2 \cdot 10^{11} \text{ cm}^{-2}$ for the measured IX energy shift in the regime of IX long-range transport $\delta E \sim 3 \text{ meV}$ ($d_z \sim 0.6 \text{ nm}$ is the separation between the electron and hole layers, $\varepsilon \sim 7.4$ is the dielectric constant [105]). $N \sim 1/2$ for this density and the moiré superlattice period $b = 17 \text{ nm}$ corresponding to the twist angle $\delta\theta = 1.1^\circ$ that agrees with the angle between MoSe₂ and WSe₂ layers in the HS ($b \sim a/\delta\theta$, a is the lattice constant). The agreement with the Bose-Hubbard model is outlined in the studies of the IX long-range transport in $B = 0$ in Ref. [85].

In this work, we extended the IX transport measurements to magnetic fields up to 8 T . We observed the IX long-range transport with the decay distance $d_{1/e}$ reaching $\sim 100 \mu\text{m}$ in the magnetic fields (Figs. 1d and 3a). We also observed that $d_{1/e}$ first enhances and then decreases with increasing IX density in the magnetic fields (Figs. 1d and 3a). The IX long-range transport and the non-monotonic IX transport dependence on density in the magnetic fields in this work are consistent with the similar IX long-range transport and the non-monotonic IX transport dependence on density in zero magnetic field in Ref. [85] and, in turn, are consistent with the Bose-Hubbard model as outlined above.

The IX transport dependences on density and on magnetic field in the MoSe₂/WSe₂ HS (Figs. 1d and 3a) are strongly different from the IX transport dependences on density and on magnetic field in GaAs/AlGaAs HS [10, 13, 94, 95]. In contrast to the monotonic enhancement of IX transport with IX density in GaAs/AlGaAs

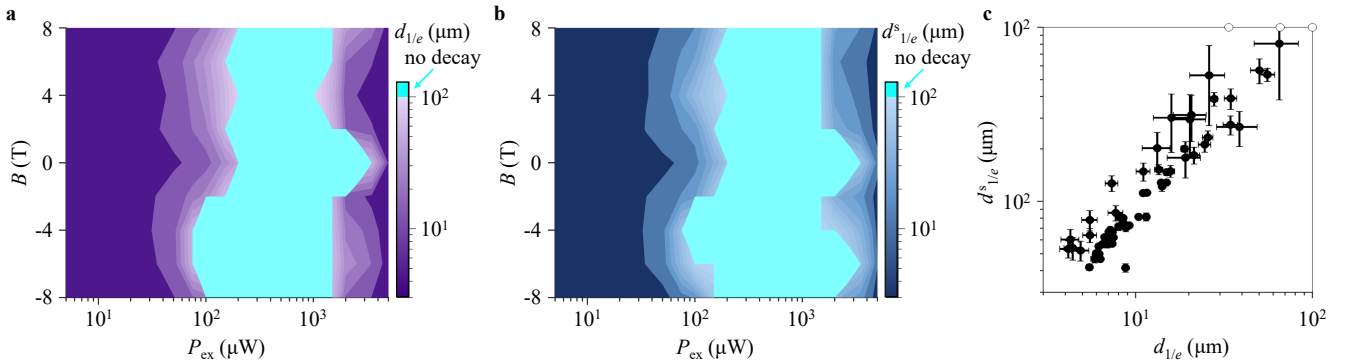


FIG. 3: **Excitation power and magnetic field dependence of IX transport and IX mediated spin transport.** (a-b) The $1/e$ decay distance of LE-IX transport $d_{1/e}$ (a) and the $1/e$ decay distance of LE-IX mediated spin density transport $d_{1/e}^s$ (b) vs. P_{ex} and B . The $d_{1/e}$ and $d_{1/e}^s$ values are obtained from least-squares fitting the LE-IX luminescence profiles and I_{spin} profiles, respectively, to exponential decays in the region $x = 0 - 9 \mu\text{m}$, from the excitation spot to the HS edge. The data with the fit indicating diverging $d_{1/e}$ (a) or $d_{1/e}^s$ (b) are presented by cyan color. (c) Correlation between $d_{1/e}^s$ and $d_{1/e}$. The values for $d_{1/e}$ and $d_{1/e}^s$ are taken from (a) and (b). The data with the fit indicating diverging $d_{1/e}^s$ and $d_{1/e}$ are presented by circles on the edge. The error bars represent the uncertainty in least-squares fitting the transport decays to exponential decays. The enhancement of $d_{1/e}^s$ with $d_{1/e}$ is observed in a broad range of both excitation density and magnetic field variations, corresponding to the range of these parameters in (a, b).

HS both in zero magnetic field [10, 13] and in magnetic fields up to 10 T [94], IX transport in the MoSe₂/WSe₂ HS non-monotonically varies with IX density in all studied magnetic fields (Figs. 1d and 3a) as outlined above. This difference is consistent with the lack of a moiré superlattice potential for IXs in GaAs/AlGaAs HS and the presence of the moiré superlattice potential for IXs in MoSe₂/WSe₂ HS: as outlined above, the transition from IX localization to IX long-range transport to IX localization with increasing IX density is in qualitative agreement with the Bose-Hubbard model prediction for superfluid and insulating phases in periodic potentials of moiré superlattices.

Furthermore, in contrast to the strong suppression of IX transport distances in GaAs/AlGaAs HS by the magnetic field [94, 95], no such suppression is observed in MoSe₂/WSe₂ HS (Figs. 1c,d). This difference is consistent with the theory of magnetoexcitons [87–93]. The IX transport in GaAs/AlGaAs HS is suppressed due to the enhancement of IX mass in the magnetic field [94, 95]. A strong enhancement of the exciton mass is realized in the high-magnetic-field regime when the cyclotron energy is comparable or larger than the exciton binding energy [87–93]. Due to the small IX binding energy and the high electron and hole cyclotron energies originating from the small electron and hole masses in GaAs/AlGaAs HS, the high-magnetic-field regime is realized in the magnetic fields ~ 10 T in GaAs/AlGaAs HS and the strong enhancement of the IX mass in these magnetic fields [92, 93] strongly suppresses the IX transport in GaAs/AlGaAs HS [94, 95]. In contrast, due to the high IX binding energy and the low electron and hole cyclotron energies originating from the large electron and

hole masses in MoSe₂/WSe₂ HS, the high-magnetic field regime is not realized in the magnetic fields ~ 10 T in MoSe₂/WSe₂ HS and neither strong enhancement of the IX mass nor strong suppression of the IX transport is expected in these magnetic fields in MoSe₂/WSe₂ HS, that is consistent with the data in Figs. 1c,d and 3a.

IX mediated spin transport. The long-range spin transport with the decay length reaching $\sim 100 \mu\text{m}$ and the correlation of the spin transport decay length $d_{1/e}^s$ with the IX transport decay length $d_{1/e}$ were observed in the studies of IX mediated spin transport in $B = 0$ in Ref. [86]. In this work, we extended the measurements of IX mediated spin transport to magnetic fields up to 8 T. We observed the long-range spin transport with the decay length reaching $\sim 100 \mu\text{m}$ in the magnetic fields (Figs. 2d, 3b). We also observed the correlation of the spin transport decay length with the IX transport decay length in the magnetic fields (Fig. 3c). The long-range spin transport and its correlation with the IX transport in the magnetic fields are consistent with the similar long-range spin transport and its correlation with the IX transport in zero magnetic field in Ref. [86]. The correlation of the longer-range spin transport with the longer-range IX transport and, in turn, with the suppressed IX scattering complies with the suppression of the spin relaxation due to the suppression of scattering of particles carrying the spin states [4].

CONCLUSION

We studied transport of IXs and IX mediated spin transport in a MoSe₂/WSe₂ heterostructure in magnetic

fields up to 8 T. We observed the long-range IX transport and the long-range IX mediated spin transport with the $1/e$ decay distances reaching $\sim 100 \mu\text{m}$ in the magnetic fields. The decay distance of the spin transport correlates with the decay distance of IX transport. These decay distances first increase and then decrease with increasing IX density in the magnetic fields. The long-range IX transport and the long-range IX mediated spin transport in the magnetic fields are consistent with the similar long-range transport in zero magnetic field.

ACKNOWLEDGMENTS

We thank Misha Fogler for discussions. The experiments were supported by the Department of Energy, Office of Basic Energy Sciences, under award DE-FG02-07ER46449. The heterostructure manufacturing was supported by NSF Grant 1905478. The data analysis was supported by NSF Grant 2516006.

APPENDIX A: HETEROSTRUCTURE

The MoSe₂/WSe₂ HS was assembled using the dry-transfer peel technique [97]. The HS manufacturing details are described in Ref. [85]. The same HS was used for studies of IX transport in Ref. [85] and for studies of IX mediated spin transport in Ref. [86] in zero magnetic field. The thickness of the bottom hBN layer is $\sim 40 \text{ nm}$, the thickness of the top hBN layer is $\sim 30 \text{ nm}$. The MoSe₂ monolayer is on top of the WSe₂ monolayer. The hBN layers cover the entire areas of MoSe₂ and WSe₂ layers. The WSe₂ and MoSe₂ edges were used for a rotational alignment between the WSe₂ and MoSe₂ monolayers. The twist angle between the monolayers $\delta\theta = 1.1^\circ$ corresponding to the moiré superlattice period $b = 17 \text{ nm}$ agrees with the angle between MoSe₂ and WSe₂ edges in the HS [85, 86]. The moiré potentials can be affected by atomic reconstruction [98–100] and by disorder and may vary over the HS area. The measured IX g-factor ~ -16 corresponds to H stacking in the MoSe₂/WSe₂ HS [44, 101].

APPENDIX B: MEASUREMENTS

Excitons were generated by a cw Ti:Sapphire laser with the excitation energy $E_{\text{ex}} = 1.689 \text{ eV}$ resonant to DX in WSe₂ HS layer. PL spectra were measured using a spectrometer with a resolution of 0.2 meV and a liquid-nitrogen-cooled CCD. Representative polarization-resolved IX PL spectra are presented in Appendix C. The spatial profiles of polarization-resolved IX PL vs. x were obtained from the polarization-resolved PL images detected using the CCD with the spa-

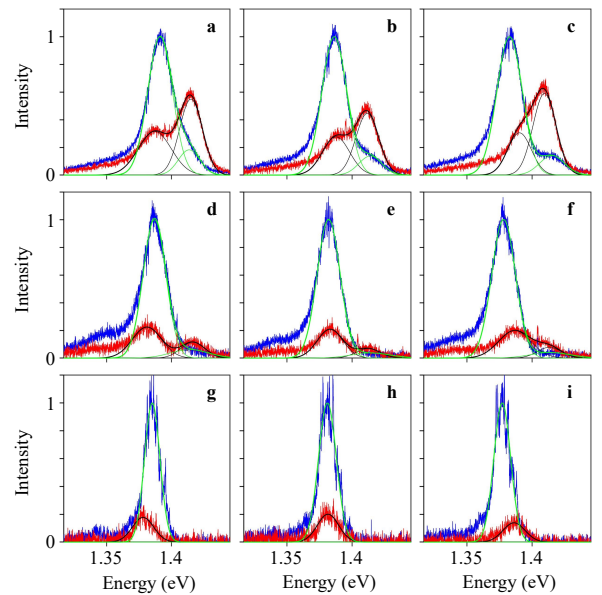


FIG. 4: IX PL spectra. Co-polarized (blue) and cross-polarized (red) IX spectra for the excitation power $P_{\text{ex}} = 5 \text{ mW}$ (a,b,c), 500 mW (d,e,f), and $5 \mu\text{W}$ (g,h,i) in magnetic field $B = -8 \text{ T}$ (a,d,g), 0 (b,e,h) , and 8 T (c,f,i). The lower-energy IX (LE-IX) PL is co-polarized. The higher-energy IX (HE-IX) PL is cross-polarized. The HE-IXs appear in the spectra at high P_{ex} . PL spectra are normalized to the maximum of the co-polarized intensity. The Gaussian fits to the co-polarized (cross-polarized) LE-IX spectra and HE-IX spectra are shown by the thin green (black) lines. The sum of the Gaussians shown by the thin green (black) lines is shown by the thick green (black) line.

tial resolution $0.8 \mu\text{m}$. The signal was integrated within $1 \mu\text{m}$ in y direction. For a direct comparison with earlier measurements in zero magnetic field in Refs. [85, 86], IX transport and IX mediated spin transport in magnetic fields were studied along the same path.

The measurements were performed in an optical dilution refrigerator at temperature 4 K and magnetic fields up to 8 T perpendicular to the HS layer plane. The sample was mounted on an Attocube xyz piezo translation stage allowing adjusting the sample position relative to a focusing lens installed inside the fridge.

APPENDIX C: IX PL SPECTRA

Figure 4 shows IX PL spectra at different laser excitation powers P_{ex} and magnetic fields B . The spectra at $B = 0$ (Fig. 4b,e,h) are similar to the corresponding zero-field spectra in Ref. [86]: A single LE-IX PL line is observed in the spectra at low P_{ex} and an additional HE-IX PL line appears in the spectra at high P_{ex} . Similar IX spectra are observed in the magnetic fields $-8 \text{ T} < B < 8 \text{ T}$ as shown for $B = -8 \text{ T}$ in Fig. 4a,d,g and for $B = 8 \text{ T}$ in Fig. 4c,f,i.

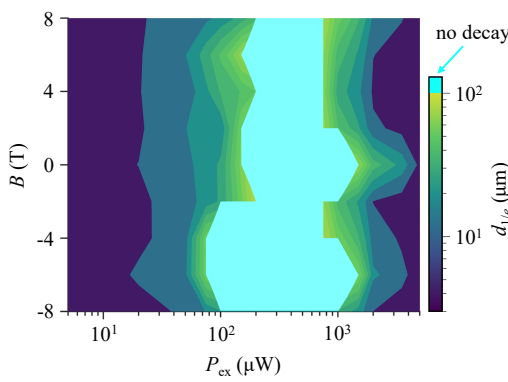


FIG. 5: EXCITATION POWER AND MAGNETIC FIELD DEPENDENCE OF IX TRANSPORT. The $1/e$ decay distance of spectrally integrated IX luminescence $d_{1/e}$ vs. P_{ex} and B . The $d_{1/e}$ values are obtained from least-squares fitting the spectrally integrated IX luminescence profiles to exponential decays in the region $x = 0 - 9 \mu\text{m}$, from the excitation spot to the HS edge. The data with the fit indicating diverging $d_{1/e}$ are presented by cyan color. Figure 5 is similar to Fig. 3a, however, Fig. 5 shows $d_{1/e}$ for the spectrally integrated IX PL including LE-IX and HE-IX, and Fig. 3a shows $d_{1/e}$ for LE-IX.

APPENDIX D: EXCITATION POWER AND MAGNETIC FIELD DEPENDENCE OF IX TRANSPORT

In the main text, we consider the propagation of the LE-IX PL intensity from the laser excitation spot to characterize the IX transport (Figs. 1-3). The LE-IX spectra are separated from the HE-IX spectra by the Gaussian fits as shown in Fig. 4. Figure 5 shows that considering the spectrally integrated IX PL intensity including both LE-IX and HE-IX gives qualitatively similar IX transport characteristics (compare Fig. 3a for LE-IX and Fig. 5 for the spectrally integrated IX PL intensity including both LE-IX and HE-IX).

[1] Y.E. Lozovik, V.I. Yudson, A new mechanism for superconductivity: pairing between spatially separated electrons and holes, *Sov. Phys. JETP* **44**, 389 (1976).

[2] A. Zrenner, P. Leeb, J. Schäfler, G. Böhm, G. Weimann, J.M. Worlock, L.T. Florez, J.P. Harbison, Indirect excitons in coupled quantum well structures, *Surf. Sci.* **263**, 496 (1992).

[3] A.A. High, J.R. Leonard, A.T. Hammack, M.M. Fogler, L.V. Butov, A.V. Kavokin, K.L. Campman, A.C. Gossard, Spontaneous coherence in a cold exciton gas, *Nature* **483**, 584 (2012).

[4] M.I. Dyakonov, *Spin Physics in Semiconductors* (Springer, New York, 2008).

[5] M.Z. Maialle, E.A. de Andrade e Silva, L.J. Sham, Exciton spin dynamics in quantum wells, *Phys. Rev. B* **47**, 15776 (1993).

[6] M. Hagn, A. Zrenner, G. Böhm, G. Weimann, Electric-field-induced exciton transport in coupled quantum well structures, *Appl. Phys. Lett.* **67**, 232 (1995).

[7] A.V. Lariionov, V.B. Timofeev, J. Hvam, K. Soerensen, Interwell Excitons in GaAs/AlGaAs Double Quantum Wells and Their Collective Properties, *J. Exp. Theor. Phys.* **90**, 1093 (2000).

[8] L.V. Butov, A.C. Gossard, D.S. Chemla, Macroscopically ordered state in an exciton system, *Nature* **418**, 751 (2002).

[9] Z. Vörös, R. Balili, D.W. Snoke, L. Pfeiffer, K. West, Long-Distance Diffusion of Excitons in Double Quantum Well Structures, *Phys. Rev. Lett.* **94**, 226401 (2005).

[10] A.L. Ivanov, L.E. Smallwood, A.T. Hammack, Sen Yang, L.V. Butov, A.C. Gossard, Origin of the inner ring in photoluminescence patterns of quantum well excitons, *Europhys. Lett.* **73**, 920 (2006).

[11] A. Gärtner, A.W. Holleitner, J.P. Kotthaus, D. Schuh, Drift mobility of long-living excitons in coupled GaAs quantum wells, *Appl. Phys. Lett.* **89**, 052108 (2006).

[12] A.A. High, E.E. Novitskaya, L.V. Butov, M. Hanson, A.C. Gossard, Control of exciton fluxes in an excitonic integrated circuit, *Science* **321**, 229 (2008).

[13] M. Remeika, J.C. Graves, A.T. Hammack, A.D. Meyert-holen, M.M. Fogler, L.V. Butov, M. Hanson, A.C. Gossard, Localization-Delocalization Transition of Indirect Excitons in Lateral Electrostatic Lattices, *Phys. Rev. Lett.* **102**, 186803 (2009).

[14] X.P. Vögele, D. Schuh, W. Wegscheider, J.P. Kotthaus, A.W. Holleitner, Density Enhanced Diffusion of Dipolar Excitons within a One-Dimensional Channel, *Phys. Rev. Lett.* **103**, 126402 (2009).

[15] S. Lazić, P.V. Santos, R. Hey, Exciton transport by moving strain dots in GaAs quantum wells, *Phys. E* **42**, 2640 (2010).

[16] M. Alloing, A. Lemaître, E. Galopin, F. Dubin, Nonlinear dynamics and inner-ring photoluminescence pattern of indirect excitons, *Phys. Rev. B* **85**, 245106 (2012).

[17] M. Remeika, M.M. Fogler, L.V. Butov, M. Hanson, A.C. Gossard, Two-dimensional electrostatic lattices for indirect excitons, *Appl. Phys. Lett.* **100**, 061103 (2012).

[18] S. Lazić, A. Violante, K. Cohen, R. Hey, R. Rapaport, P.V. Santos, Scalable interconnections for remote indirect exciton systems based on acoustic transport, *Phys. Rev. B* **89**, 085313 (2014).

[19] Mathieu Alloing, Mussie Beian, Maciej Lewenstein, David Fuster, Yolanda González, Luisa González, Roland Combescot, Monique Combescot, François Dubin, Evidence for a Bose-Einstein condensate of excitons, *Europhys. Lett.* **107**, 10012 (2014).

[20] A.V. Gorbunov, V.B. Timofeev, Coherence of Bose-Einstein condensates of dipolar excitons in GaAs/AlGaAs heterostructures, *Low. Temp. Phys.* **42**, 340 (2016).

[21] J.R. Leonard, Lunhui Hu, A.A. High, A.T. Hammack, Congjun Wu, L.V. Butov, K.L. Campman, A.C. Gossard, Moiré pattern of interference dislocations in condensate of indirect excitons, *Nat. Commun.* **12**, 1175 (2021).

[22] François Chiaruttini, Thierry Guillet, Christelle Bremont, Benoit Jouault, Pierre Lefebvre, Jessica Vives, Sébastien Chenot, Yvon Cordier, Benjamin Damilano, Maria Vladimirova, Trapping Dipolar Exciton Fluids in GaN/(AlGa)N Nanostructures, *Nano Lett.* **19**, 4911 (2019).

[23] Y.Y. Kuznetsova, F. Fedichkin, P. Andreakou, E.V. Calman, L.V. Butov, P. Lefebvre, T. Bretagnon, T. Guillet,

M. Vladimirova, C. Morhain, J.-M. Chauveau, Transport of indirect excitons in ZnO quantum wells, *Opt. Lett.* **40**, 3667 (2015).

[24] J.R. Leonard, Y.Y. Kuznetsova, Sen Yang, L.V. Butov, T. Ostatnický, A. Kavokin, A.C. Gossard, Spin Transport of Excitons, *Nano Lett.* **9**, 4204 (2009).

[25] A.A. High, A.T. Hammack, J.R. Leonard, Sen Yang, L.V. Butov, T. Ostatnický, M. Vladimirova, A.V. Kavokin, T.C.H. Liew, K.L. Campman, A.C. Gossard, Spin Currents in a Coherent Exciton Gas, *Phys. Rev. Lett.* **110**, 246403 (2013).

[26] A. Violante, R. Hey, P.V. Santos, Coherent transport and manipulation of spins in indirect-exciton nanostructures, *Phys. Rev. B* **91**, 125302 (2015).

[27] R. Finkelstein, K. Cohen, B. Jouault, K. West, L.N. Pfeiffer, M. Vladimirova, R. Rapaport, Transition from spin-orbit to hyperfine interaction dominated spin relaxation in a cold fluid of dipolar excitons, *Phys. Rev. B* **96**, 085404 (2017).

[28] J.R. Leonard, A.A. High, A.T. Hammack, M.M. Fogler, L.V. Butov, K.L. Campman, A.C. Gossard, Pancharatnam-Berry phase in condensate of indirect excitons, *Nat. Commun.* **9**, 2158 (2018).

[29] Ziliang Ye, Ting Cao, Kevin O'Brien, Hanyu Zhu, Xiaobo Yin, Yuan Wang, Steven G. Louie, Xiang Zhang, Probing excitonic dark states in single-layer tungsten disulphide, *Nature* **513**, 214 (2014).

[30] Alexey Chernikov, Timothy C. Berkelbach, Heather M. Hill, Albert Rigosi, Yilei Li, Ozgur Burak Aslan, David R. Reichman, Mark S. Hybertsen, Tony F. Heinz, Exciton Binding Energy and Nonhydrogenic Rydberg Series in Monolayer WS₂, *Phys. Rev. Lett.* **113**, 076802 (2014).

[31] M. Goryca, J. Li, A.V. Stier, T. Taniguchi, K. Watanabe, E. Courtade, S. Shree, C. Robert, B. Urbaszek, X. Marie, S.A. Crooker, Revealing exciton masses and dielectric properties of monolayer semiconductors with high magnetic fields, *Nat. Commun.* **10**, 4172 (2019).

[32] M.M. Fogler, L.V. Butov, K.S. Novoselov, High-temperature superfluidity with indirect excitons in van der Waals heterostructures, *Nat. Commun.* **5**, 4555 (2014).

[33] Thorsten Deilmann, Kristian Sommer Thygesen, Interlayer Trions in the MoS₂/WS₂ van der Waals Heterostructure, *Nano Lett.* **18**, 1460 (2018).

[34] K. Sivalertporn, L. Mouchliadis, A.L. Ivanov, R. Philp, E.A. Muljarov, Direct and indirect excitons in semiconductor coupled quantum wells in an applied electric field, *Phys. Rev. B* **85**, 045207 (2012).

[35] E.A. Szwed, B. Vermilyea, D.J. Choksy, Zhiwen Zhou, M.M. Fogler, L.V. Butov, D.K. Efimkin, K.W. Baldwin, L. Pfeiffer, Excitonic Bose Polarons in Electron-Hole Bilayers, *Nano Lett.* **24**, 13219 (2024).

[36] C. Morhain, T. Bretagnon, P. Lefebvre, X. Tang, P. Valvin, T. Guillet, B. Gil, T. Taliercio, M. Teisseire-Doninelli, B. Vinter, C. Deparis, Internal electric field in wurtzite ZnO/Zn_{0.78}Mg_{0.22}O quantum wells, *Phys. Rev. B* **72**, 241305(R) (2005).

[37] Fengcheng Wu, Timothy Lovorn, A.H. MacDonald, Theory of optical absorption by interlayer excitons in transition metal dichalcogenide heterobilayers, *Phys. Rev. B* **97**, 035306 (2018).

[38] Hongyi Yu, Gui-Bin Liu, Wang Yao, Brightened spin-triplet interlayer excitons and optical selection rules in van der Waals heterobilayers, *2D Mater.* **5**, 035021 (2018).

[39] Fengcheng Wu, Timothy Lovorn, A.H. MacDonald, Topological Exciton Bands in Moiré Heterojunctions, *Phys. Rev. Lett.* **118**, 147401 (2017).

[40] Hongyi Yu, Gui-Bin Liu, Jianju Tang, Xiaodong Xu, Wang Yao, Moiré excitons: From programmable quantum emitter arrays to spin-orbit-coupled artificial lattices, *Sci. Adv.* **3**, e1701696 (2017).

[41] Chendong Zhang, Chih-Piao Chu, Xibiao Ren, Ming-Yang Li, Lain-Jong Li, Chuanhong Jin, Mei-Yin Chou, Chih-Kang Shih, Interlayer couplings, Moiré patterns, and 2D electronic superlattices in MoS₂/WSe₂ heterobilayers, *Sci. Adv.* **3**, e1601459 (2017).

[42] Nan Zhang, Alessandro Surrenti, Michał Baranowski, Duncan K. Maude, Patricia Gant, Andres Castellanos-Gomez, Paulina Plochocka, Moiré Intralayer Excitons in a MoSe₂/MoS₂ Heterostructure, *Nano Lett.* **18**, 7651 (2018).

[43] Alberto Ciarrocchi, Dmitrii Unuchek, Ahmet Avsar, Kenji Watanabe, Takashi Taniguchi, Andras Kis, Polarization switching and electrical control of interlayer excitons in two-dimensional van der Waals heterostructures, *Nat. Photonics* **13**, 131 (2019).

[44] Kyle L. Seyler, Pasqual Rivera, Hongyi Yu, Nathan P. Wilson, Essance L. Ray, David G. Mandrus, Jiaqiang Yan, Wang Yao, Xiaodong Xu, Signatures of moiré-trapped valley excitons in MoSe₂/WSe₂ heterobilayers, *Nature* **567**, 66 (2019).

[45] Kha Tran, Galan Moody, Fengcheng Wu, Xiaobo Lu, Junho Choi, Kyoungwan Kim, Amritesh Rai, Daniel A. Sanchez, Jiamin Quan, Akshay Singh, Jacob Embrey, André Zepeda, Marshall Campbell, Travis Autry, Takashi Taniguchi, Kenji Watanabe, Nanshu Lu, Sanjay K. Banerjee, Kevin L. Silverman, Suenne Kim, Emanuel Tutuc, Li Yang, Allan H. MacDonald, Xiaoqin Li, Evidence for moiré excitons in van der Waals heterostructures, *Nature* **567**, 71 (2019).

[46] Chenhao Jin, Emma C. Regan, Aiming Yan, M. Iqbal Bakti Utama, Danqing Wang, Sihan Zhao, Ying Qin, Si-jie Yang, Zhiren Zheng, Shenyang Shi, Kenji Watanabe, Takashi Taniguchi, Sefaattin Tongay, Alex Zettl, Feng Wang, Observation of moiré excitons in WSe₂/WS₂ heterostructure superlattices, *Nature* **567**, 76 (2019).

[47] Evgeny M. Alexeev, David A. Ruiz-Tijerina, Mark Danovich, Matthew J. Hamer, Daniel J. Terry, Pramoda K. Nayak, Seongjoon Ahn, Sangyeon Pak, Juwon Lee, Jung Inn Sohn, Maciej R. Molas, Maciej Koperski, Kenji Watanabe, Takashi Taniguchi, Kostya S. Novoselov, Roman V. Gorbachev, Hyeyon Suk Shin, Vladimir I. Fal'ko, Alexander I. Tartakovskii, Resonantly hybridized excitons in moiré superlattices in van der Waals heterostructures, *Nature* **567**, 81 (2019).

[48] Chenhao Jin, Emma C. Regan, Danqing Wang, M. Iqbal Bakti Utama, Chan-Shan Yang, Jeffrey Cain, Ying Qin, Yuxia Shen, Zhiren Zheng, Kenji Watanabe, Takashi Taniguchi, Sefaattin Tongay, Alex Zettl, Feng Wang, Identification of spin, valley and moiré quasi-angular momentum of interlayer excitons, *Nat. Phys.* **15**, 1140 (2019).

[49] Yuya Shimazaki, Ido Schwartz, Kenji Watanabe, Takashi Taniguchi, Martin Kröner, Ataç Imamoğlu, Strongly correlated electrons and hybrid excitons in a moiré heterostructure, *Nature* **580**, 472 (2020).

[50] Nathan P. Wilson, Wang Yao, Jie Shan, Xiaodong Xu, Excitons and emergent quantum phenomena in stacked 2D semiconductors, *Nature* **599**, 383 (2021).

[51] Jie Gu, Liguo Ma, Song Liu, Kenji Watanabe, Takashi

Taniguchi, James C. Hone, Jie Shan, Kin Fai Mak, Dipolar excitonic insulator in a moiré lattice, *Nat. Phys.* **18**, 395 (2022).

[52] Nardeep Kumar, Qiannan Cui, Frank Ceballos, Dawei He, Yongsheng Wang, Hui Zhao, Exciton diffusion in monolayer and bulk MoSe₂, *Nanoscale* **6**, 4915, (2014).

[53] Marvin Kulig, Jonas Zipfel, Philipp Nagler, Sofia Blanter, Christian Schüller, Tobias Korn, Nicola Paradiso, Mikhail M. Glazov, Alexey Chernikov, Exciton Diffusion and Halo Effects in Monolayer Semiconductors, *Phys. Rev. Lett.* **120**, 207401 (2018).

[54] F. Cadiz, C. Robert, E. Courtade, M. Manca, L. Martinelli, T. Taniguchi, K. Watanabe, T. Amand, A.C.H. Rowe, D. Paget, B. Urbaszek, X. Marie, Exciton diffusion in WSe₂ monolayers embedded in a van der Waals heterostructure, *Appl. Phys. Lett.* **112**, 152106 (2018).

[55] Darwin F. Cordovilla Leon, Zidong Li, Sung Woon Jang, Che-Hsuan Cheng, Parag B. Deotare, Exciton transport in strained monolayer WSe₂, *Appl. Phys. Lett.* **113**, 252101 (2018).

[56] Darwin F. Cordovilla Leon, Zidong Li, Sung Woon Jang, Parag B. Deotare, Hot exciton transport in WSe₂ monolayers, *Phys. Rev. B* **100**, 241401(R) (2019).

[57] Shengcai Hao, Matthew Z. Bellus, Dawei He, Yongsheng Wang, Hui Zhao, Controlling exciton transport in monolayer MoSe₂ by dielectric screening, *Nanoscale Horiz.* **5**, 139 (2020).

[58] Kanak Datta, Zhengyang Lyu, Zidong Li, Takashi Taniguchi, Kenji Watanabe, Parag B. Deotare, Spatiotemporally controlled room-temperature exciton transport under dynamic strain, *Nat. Photonics* **16**, 242 (2022).

[59] Pasqual Rivera, Kyle L. Seyler, Hongyi Yu, John R. Schaibley, Jiaqiang Yan, David G. Mandrus, Wang Yao, Xiaodong Xu, Valley-polarized exciton dynamics in a 2D semiconductor heterostructure, *Science* **351**, 688 (2016).

[60] Luis A. Jauregui, Andrew Y. Joe, Kateryna Pistunova, Dominik S. Wild, Alexander A. High, You Zhou, Giovanni Scuri, Kristiaan De Greve, Andrey Sushko, Che-Hang Yu, Takashi Taniguchi, Kenji Watanabe, Daniel J. Needleman, Mikhail D. Lukin, Hongkun Park, Philip Kim, Electrical control of interlayer exciton dynamics in atomically thin heterostructures, *Science* **366**, 870 (2019).

[61] Dmitrii Unuchek, Alberto Ciarrocchi, Ahmet Avsar, Kenji Watanabe, Takashi Taniguchi, Andras Kis, Room-temperature electrical control of exciton flux in a van der Waals heterostructure, *Nature* **560**, 340 (2019).

[62] Dmitrii Unuchek, Alberto Ciarrocchi, Ahmet Avsar, Zhe Sun, Kenji Watanabe, Takashi Taniguchi, Andras Kis, Valley-polarized exciton currents in a van der Waals heterostructure, *Nat. Nanotechnol.* **14**, 1104 (2019).

[63] Yuanda Liu, Kévin Dini, Qinghai Tan, Timothy Liew, Kostya S. Novoselov, Weibo Gao, Electrically controllable router of interlayer excitons, *Sci. Adv.* **6**, eaba1830 (2020).

[64] Junho Choi, Wei-Ting Hsu, Li-Syuan Lu, Liuyang Sun, Hui-Yu Cheng, Ming-Hao Lee, Jiamin Quan, Kha Tran, Chun-Yuan Wang, Matthew Staab, Kayleigh Jones, Takashi Taniguchi, Kenji Watanabe, Ming-Wen Chu, Shangir Gwo, Suenne Kim, Chih-Kang Shih, Xiaoqin Li, Wen-Hao Chang, Moiré potential impedes interlayer exciton diffusion in van der Waals heterostructures, *Sci. Adv.* **6**, eaba8866 (2020).

[65] Zumeng Huang, Yuanda Liu, Kevin Dini, Qinghai Tan, Zhuojun Liu, Hanlin Fang, Jin Liu, Timothy Liew, Weibo Gao, Robust room temperature valley Hall effect of interlayer excitons, *Nano Lett.* **20**, 1345 (2020).

[66] Long Yuan, Biyuan Zheng, Jens Kunstmüller, Thomas Brumme, Agnieszka Beata Kuc, Chao Ma, Shabin Deng, Daria Blach, Anlian Pan, Libai Huang, Twist-angle-dependent interlayer exciton diffusion in WS₂-WSe₂ heterobilayers, *Nat. Mater.* **19**, 617 (2020).

[67] Zidong Li, Xiaobo Lu, Darwin F. Cordovilla Leon, Zhengyang Lyu, Hongchao Xie, Jize Hou, Yanzhao Lu, Xiaoyu Guo, Austin Kaczmarek, Takashi Taniguchi, Kenji Watanabe, Liuyan Zhao, Li Yang, Parag B. Deotare, Interlayer Exciton Transport in MoSe₂/WSe₂ Heterostructures, *ACS Nano* **15**, 1539 (2021).

[68] Jue Wang, Qianhui Shi, En-Min Shih, Lin Zhou, Wenjing Wu, Yusong Bai, Daniel Rhodes, Katayun Barmak, James Hone, Cory R. Dean, X.-Y. Zhu, Diffusivity Reveals Three Distinct Phases of Interlayer Excitons in MoSe₂/WSe₂ Heterobilayers, *Phys. Rev. Lett.* **126**, 106804 (2021).

[69] Daniel N. Shanks, Fateme Mahdikhany Sarvejehany, Trevor G. Stanfill, Michael R. Koehler, David G. Mandrus, Takashi Taniguchi, Kenji Watanabe, Brian J. LeRoy, John R. Schaibley, Interlayer Exciton Diode and Transistor, *Nano Lett.* **22**, 6599 (2022).

[70] Zhe Sun, Alberto Ciarrocchi, Fedele Tagarelli, Juan Francisco Gonzalez Marin, Kenji Watanabe, Takashi Taniguchi, Andras Kis, Excitonic transport driven by repulsive dipolar interaction in a van der Waals heterostructure, *Nat. Photonics* **16**, 79 (2022).

[71] Fedele Tagarelli, Edoardo Lopriore, Daniel Erkensten, Raúl Perea-Causín, Samuel Brem, Joakim Hagel, Zhe Sun, Gabriele Pasquale, Kenji Watanabe, Takashi Taniguchi, Ermin Malic, Andras Kis, Electrical control of hybrid exciton transport in a van der Waals heterostructure, *Nat. Photonics* **17**, 615 (2023).

[72] Antonio Rossi, Jonas Zipfel, Indrajit Maity, Monica Lorenzon, Luca Francaviglia, Emma C. Regan, Zuocheng Zhang, Jacob H. Nie, Edward Barnard, Kenji Watanabe, Takashi Taniguchi, Eli Rotenberg, Feng Wang, Johannes Lischner, Archana Raja, Alexander Weber-Bargioni, Phason-mediated interlayer exciton diffusion in WS₂/WSe₂ moiré heterostructure, arXiv:2301.07750 (2023).

[73] Beini Gao, Daniel G. Suárez-Forero, Supratik Sarkar, Tsung-Sheng Huang, Deric Session, Mahmoud Jalali Mehrabad, Ruihao Ni, Ming Xie, Pranshoo Upadhyay, Jonathan Vannucci, Sunil Mittal, Kenji Watanabe, Takashi Taniguchi, Atac Imamoglu, You Zhou, Mohammad Hafezi, Excitonic Mott insulator in a Bose-Fermi-Hubbard system of moiré WS₂/WSe₂ heterobilayer, *Nat. Commun.* **15**, 2305 (2024).

[74] Lifu Zhang, Liuxin Gu, Ruihao Ni, Ming Xie, Suji Park, Houk Jang, Rundong Ma, Takashi Taniguchi, Kenji Watanabe, You Zhou, Electrical Control and Transport of Tightly Bound Interlayer Excitons in a MoSe₂/hBN/MoSe₂ Heterostructure, *Phys. Rev. Lett.* **132**, 216903 (2024).

[75] Edith Wietek, Matthias Florian, Jonas Göser, Takashi Taniguchi, Kenji Watanabe, Alexander Högele, Mikhail M. Glazov, Alexander Steinhoff, Alexey Chernikov, Non-linear and Negative Effective Diffusivity of Interlayer Excitons in Moiré-Free Heterobilayers, *Phys. Rev. Lett.* **132**, 016202 (2024).

[76] L.H. Fowler-Gerace, D.J. Choksy, L.V. Butov, Voltage-controlled long-range propagation of indirect excitons in a van der Waals heterostructure, *Phys. Rev. B* **104**, 165302

(2021).

[77] Ruoming Peng, Adina Ripin, Yusen Ye, Jiayi Zhu, Changming Wu, Seokhyeong Lee, Huan Li, Takashi Taniguchi, Kenji Watanabe, Ting Cao, Xiaodong Xu, Mo Li, Long-range transport of 2D excitons with acoustic waves, *Nat. Commun.* **13**, 1334 (2022).

[78] Mirco Troue, Johannes Figueiredo, Lukas Sigl, Christos Paspalides, Manuel Katzer, Takashi Taniguchi, Kenji Watanabe, Malte Selig, Andreas Knorr, Ursula Wurstbauer, Alexander W. Holleitner, Extended Spatial Coherence of Interlayer Excitons in MoSe₂/WSe₂ Heterobilayers, *Phys. Rev. Lett.* **131**, 036902 (2023).

[79] Jacob Cutshall, Fateme Mahdikhany, Anna Roche, Daniel N. Shanks, Michael R. Koehler, David G. Mandrus, Takashi Taniguchi, Kenji Watanabe, Qizhong Zhu, Brian J. LeRoy, John R. Schaibley, Imaging interlayer exciton superfluidity in a 2D semiconductor heterostructure, *Sci. Adv.* **11**, eadir1772 (2025).

[80] Masaru Onga, Yijin Zhang, Toshiya Ideue, Yoshihiro Iwasa, Exciton Hall effect in monolayer MoS₂, *Nat. Mater.* **16**, 1193 (2017).

[81] Di Xiao, Gui-Bin Liu, Wanxiang Feng, Xiaodong Xu, Wang Yao, Coupled Spin and Valley Physics in Monolayers of MoS₂ and Other Group-VI Dichalcogenides, *Phys. Rev. Lett.* **108**, 196802 (2012).

[82] Ting Cao, Gang Wang, Wenpeng Han, Huiqi Ye, Chuanrui Zhu, Junren Shi, Qian Niu, Pingheng Tan, Enge Wang, Baoli Liu, Ji Feng, Valley-selective circular dichroism of monolayer molybdenum disulphide, *Nat. Commun.* **3**, 887 (2012).

[83] Hualing Zeng, Junfeng Dai, Wang Yao, Di Xiao, Xiaodong Cui, Valley polarization in MoS₂ monolayers by optical pumping, *Nat. Nanotechnol.* **7**, 490 (2012).

[84] Kin Fai Mak, Keliang He, Jie Shan, Tony F. Heinz, Control of valley polarization in monolayer MoS₂ by optical helicity, *Nat. Nanotechnol.* **7**, 494 (2012).

[85] L.H. Fowler-Gerace, Zhiwen Zhou, E.A. Szwed, D.J. Choksy, L.V. Butov, Transport and localization of indirect excitons in a van der Waals heterostructure, *Nat. Photonics* **18**, 823 (2024).

[86] Zhiwen Zhou, E.A. Szwed, D.J. Choksy, L.H. Fowler-Gerace, L.V. Butov, Long-distance decay-less spin transport in indirect excitons in a van der Waals heterostructure, *Nat. Commun.* **15**, 9454 (2024).

[87] L.P. Gor'kov, I.E. Dzyaloshinskii, Contribution to the theory of the Mott exciton in a strong magnetic field, *Sov. Phys. JETP* **26**, 449 (1968).

[88] I.V. Lerner, Yu.E. Lozovik, Mott exciton in a quasi-two-dimensional semiconductor in a strong magnetic field, *Sov. Phys. JETP* **51**, 588 (1980).

[89] C. Kallin, B.I. Halperin, Excitations from a filled Landau level in the two-dimensional electron gas, *Phys. Rev. B* **30**, 5655 (1984).

[90] D. Paquet, T.M. Rice, K. Ueda, Two-dimensional electron-hole fluid in a strong perpendicular magnetic field: Exciton Bose condensate or maximum density two-dimensional droplet, *Phys. Rev. B* **32**, 5208 (1985).

[91] Yu.E. Lozovik, A.M. Ruvinskii, Magnetoexciton absorption in coupled quantum wells, *JETP* **85**, 979 (1997).

[92] L.V. Butov, C.W. Lai, D.S. Chemla, Yu.E. Lozovik, K.L. Campman, A.C. Gossard, Observation of Magnetically Induced Effective-Mass Enhancement of Quasi-2D Excitons, *Phys. Rev. Lett.* **87**, 216804 (2001).

[93] Yu.E. Lozovik, I.V. Ovchinnikov, S.Yu. Volkov, L.V. Butov, D.S. Chemla, Quasi-two-dimensional excitons in finite magnetic fields, *Phys. Rev. B* **65**, 235304 (2002).

[94] Y.Y. Kuznetsova, C.J. Dorow, E.V. Calman, L.V. Butov, J. Wilkes, E.A. Muljarov, K.L. Campman, A.C. Gossard, Transport of indirect excitons in high magnetic fields, *Phys. Rev. B* **95**, 125304 (2017).

[95] C.J. Dorow, M.W. Hasling, E.V. Calman, L.V. Butov, J. Wilkes, K.L. Campman, A.C. Gossard, Spatially resolved and time-resolved imaging of transport of indirect excitons in high magnetic fields, *Phys. Rev. B* **95**, 235308 (2017).

[96] Pasqual Rivera, John R. Schaibley, Aaron M. Jones, Jason S. Ross, Sanfeng Wu, Grant Aivazian, Philip Clement, Kyle Seyler, Genevieve Clark, Nirmal J. Ghimire, Jiaqiang Yan, D.G. Mandrus, Wang Yao, Xiaodong Xu, Observation of long-lived interlayer excitons in monolayer MoSe₂-WSe₂ heterostructures, *Nat. Commun.* **6**, 6242 (2015).

[97] F. Withers, O. Del Pozo-Zamudio, A. Mishchenko, A.P. Rooney, A. Gholinia, K. Watanabe, T. Taniguchi, S.J. Haigh, A.K. Geim, A.I. Tartakovskii, K.S. Novoselov, Light-emitting diodes by band-structure engineering in van der Waals heterostructures, *Nat. Mater.* **14**, 301 (2015).

[98] Astrid Weston, Yichao Zou, Vladimir Enaldiev, Alex Summerfield, Nicholas Clark, Viktor Zolyomi, Abigail Graham, Celal Yelgel, Samuel Magorrian, Mingwei Zhou, Johanna Zultak, David Hopkinson, Alexei Barinov, Thomas H. Bointon, Andrey Kretinin, Neil R. Wilson, Peter H. Beton, Vladimir I. Fal'ko, Sarah J. Haigh, Roman Gorbachev, Atomic reconstruction in twisted bilayers of transition metal dichalcogenides, *Nat. Nanotechnol.* **15**, 592 (2020).

[99] Matthew R. Rosenberger, Hsun-Jen Chuang, Madeleine Phillips, Vladimir P. Oleshko, Kathleen M. McCreary, Saujan V. Sivaram, C. Stephen Hellberg, Berend T. Jonker, Twist Angle-Dependent Atomic Reconstruction and Moiré Patterns in Transition Metal Dichalcogenide Heterostructures, *ACS Nano* **14**, 4550 (2020).

[100] Shen Zhao, Zhijie Li, Xin Huang, Anna Rupp, Jonas Göser, Ilia A. Vovk, Stanislav Yu. Kruchinin, Kenji Watanabe, Takashi Taniguchi, Ismail Bilgin, Anvar S. Baimuratov, Alexander Högele, Excitons in mesoscopically reconstructed moiré heterostructures, *Nat. Nanotechnol.* **18**, 572 (2023).

[101] Tomasz Woźniak, Paulo E. Faria Junior, Gotthard Seifert, Andrey Chaves, Jens Kunstmänn, Exciton g factors of van der Waals heterostructures from first-principles calculations, *Phys. Rev. B* **101**, 235408 (2020).

[102] A.L. Ivanov, Quantum diffusion of dipole-oriented indirect excitons in coupled quantum wells, *Europhys. Lett.* **59**, 586 (2002).

[103] Matthew P.A. Fisher, Peter B. Weichman, G. Grinstein, Daniel S. Fisher, Boson localization and the superfluid-insulator transition, *Phys. Rev. B* **40**, 546 (1989).

[104] Daijiro Yoshioka, Allan H. MacDonald, Double quantum well electron-hole systems in strong magnetic fields, *J. Phys. Soc. Jpn.* **59**, 4211 (1990).

[105] Akash Laturia, Maarten L. Van de Put, William G. Vandenberghe, Dielectric properties of hexagonal boron nitride and transition metal dichalcogenides: from monolayer to bulk, *npj 2D Mater. Appl.* **2**, 6 (2018).